The following publication Zian Wang, Tianshun Zhang, Yin Xiao, Zhigang Liu, and Wen Chen, "Common-path ghost imaging through complex media with dual polarization," Opt. Lett. 50, 1152-1155 (2025) is available at https://doi.org/10.1364/OL.553837.

Common-path ghost imaging through complex media with dual polarization

ZIAN WANG,[1,2] TIANSHUN ZHANG,[1] YIN XIAO,[1] ZHIGANG LIU,[2,3] AND WEN CHEN[1,*]

[1]*Department of Electrical and Electronic Engineering, The Hong Kong Polytechnic University, Hong Kong, China*
[2]*State Key Laboratory of Education Ministry for Modern Design and Rotor-Bearing System, Xi'an Jiaotong University, Xi'an Shaanxi, China*
[3]*mezgliu@mail.xjtu.edu.cn*
**owen.chen@polyu.edu.hk*

The performance of ghost imaging (GI) is severely compromised by dynamic and complex scattering media in free space. In this Letter, we design a common-path GI (CPGI) setup with dual polarization in complex environments. The s-light and p-light with mutually perpendicular polarization states are generated, and overlap in free space in the designed optical path to correct a series of dynamic scaling factors induced by the complex scattering media. Experimental results demonstrate that the proposed method is highly robust, and can achieve high imaging quality in complex media. Compared to previous schemes, the proposed method adopts a simplified optical setup, and realizes high-quality GI in complex and dynamic scattering environments without extra algorithms in order to promote the wider application of GI.

Scattering media could cause irregular motions of photons, making optical imaging to be ineffective [1,2]. It has been demonstrated that ghost imaging (GI) [3] can be applied to effectively mitigate the effect of scattering media, thus enhancing imaging quality [4,5]. The applications of GI [6–13] span across remote sensing, radar systems, 3D imaging, spectral imaging, optical encryption and biological imaging etc. Despite these advantages, in the presence of complex and dynamic scattering media, a series of dynamic scaling factors induced by the media disrupt beam correlation, ultimately compromising the potential of GI [14,15].

The current developments in GI mainly consist of algorithm design and optical design [14–25]. Sun et al. [20] combined the offset-position pseudo-Bessel-ring and speckle patterns to improve quality of the GI. The temporally-corrected GI [14] was introduced so that dynamic scaling factors can be corrected to realize object reconstruction. Recently, neural networks have garnered much interest to be used to withstand scattering media [23,24]. However, the high complexity of the algorithms could pose a significant barrier to the practical implementation of GI, leading to the usage of huge time especially for the deep learning-based GI through complex and dynamic scattering media. Regarding optical designs, Shi et al. [17] introduced adaptive GI to enhance imaging resolution amidst atmospheric turbulence. Yu et al. [19] decomposed the changes within scattering media and used Monte Carlo model to emulate light behavior in foggy conditions. We designed a dual-arm optical setup [26] to mitigate the effect of dynamic scaling factors in complex and dynamic scattering media. However, the complexity and robustness of optical structures could still be considered as a challenge. For instance, to realize high-resolution imaging, the number of elements in the adaptive mirror system must be increased [17], leading to high complexity. The designed optical setup [26] could affect GI quality under the influence of strong interference through scattering media. The influence may also arise from the interference of linearly polarized lights in horizontal and vertical components [19].

In this Letter, we design a common-path GI (CPGI) setup with dual polarization in complex scattering environments. The s-light and p-light with mutually perpendicular polarization states are generated, and overlap in free space in the designed optical path. With this optical design, a common path is applied so that the same dynamic scaling factors can be created in complex scattering environments at each instant. Compared to the existing schemes, the proposed system has a simplified optical setup, enabling high-quality GI in dynamic and complex scattering environments with a

low consumption of computational resource (e.g., no need of extra algorithms).

The principle of the proposed CPGI with dual polarization is shown in Fig. 1. After propagating through a polarization beam splitter (PBS1), the laser is divided into two beams with mutually perpendicular polarization states, respectively termed as s-light and p-light, and a quarter wave plate (QWP) is used to adjust light intensities. An amplitude-only SLM is sequentially loaded with a series of pre-generated random patterns (R) to dynamically modulate the p-light at each instant i. At the same time, the s-light is reflected by a mirror. The two beams are directed towards a sample O, then passing through complex scattering media. Finally, the two beams are separated by PBS2, and a series of single-pixel light intensities are recorded as I_{pi} and I_{si} using BD1 and BD2, respectively.

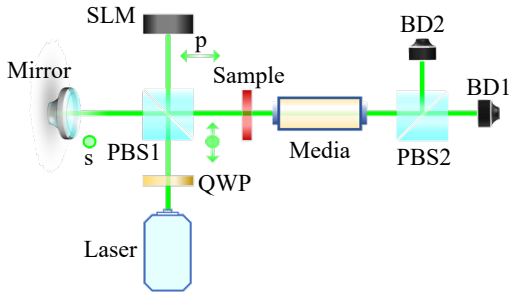

Fig. 1. A schematic of the developed CPGI with dual polarization in dynamic and complex scattering media. PBS: Polarization beam splitter; QWP: Quarter wave plate; BD: Single-pixel bucket detector.

At each instant i, the collected single-pixel light intensities (I_{si} and I_{pi}) in the s-light and p-light paths can be respectively described by

$$I_{si} = \lambda_{si} \int L(x,y) O(x,y) dxdy, \tag{1}$$

$$I_{pi} = \lambda_{pi} \int R_i(x,y) O(x,y) dxdy, \tag{2}$$

where $L(x,y)$ denotes a fixed pattern, $O(x,y)$ denotes a sample, and λ_{si} and λ_{pi} denote the induced dynamic scaling factors in the s-light and p-light paths through complex media, respectively. Since a common path is designed in the optical setup, we can have

$$\lambda_{si} \approx \lambda_{pi}. \tag{3}$$

Therefore, the series of dynamic scaling factors induced by complex scattering media can be removed as described by

$$I_{ci} = \frac{I_{pi}}{I_{si}} = \frac{1}{a} \int R_i(x,y) O(x,y) dxdy, \tag{4}$$

$$a = \int L(x,y) O(x,y) dxdy, \tag{5}$$

where I_{ci} denotes a series of corrected single-pixel light intensities. Finally, a reconstructed ghost image $\hat{O}(x,y)$ is obtained by using the correlation algorithm as described by

$$\hat{O}(x,y) = \left\langle \left(aI_{ci} - \langle aI_{ci} \rangle \right) \left(R_i - \langle R_i \rangle \right) \right\rangle, \tag{6}$$

where $\langle\ \rangle$ denotes an ensemble averaging. Since parameter a is constant, it can be omitted. The aforementioned process constitutes the principle of the designed CPGI with dual polarization.

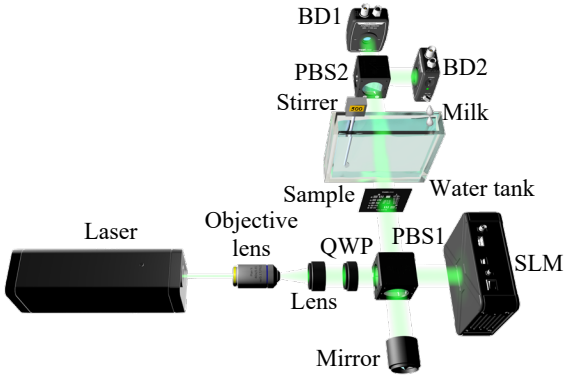

Fig. 2. Schematic of an experimental setup to verify the designed CPGI with dual polarization in dynamic and complex scattering media. Two lenses with the same focal length of 150.0 mm are used as a 4f system between the SLM and sample, not shown for the sake of brevity.

To verify feasibility and effectiveness of the proposed CPGI with dual polarization, dynamic and complex scenes with varying parameters were employed in a series of optical experiments. As shown in Fig. 2, a green laser with wavelength of 532.0 nm (CrystaLaser, CL532-025-S) was expanded by an objective lens (40×) and collimated to illuminate amplitude-only SLM with pixel size of 4.5 μm. The SLM was sequentially loaded with 16384 random patterns (1024×1024 pixels) to be projected onto a sample, i.e., the USAF 1951 resolution target (Thorlabs, R3L3S1N). Here, original patterns with 128×128 pixels were linearly interpolated 8 times to be 1024×1024 pixels in order to satisfy the experimental requirements. Then, the light beams propagated through water tank (10.0 cm (length) × 15.0 cm (width) × 30.0 cm (height)) filled with 3000-ml clean water at each experiment. A specific volume of skimmed milk was diluted with 200-ml clean water to be continuously dripped into water tank in each experiment, and a stirrer is used to create a dynamic scattering environment. At the detection plane, two single-pixel detectors (Thorlabs, PDA100A2) were simultaneously utilized to sequentially collect a series of single-pixel light intensities in the s-light and p-light paths, respectively.

Figures 3(a) and 3(b) show the reconstructed object images obtained by using conventional GI and the proposed CPGI with dual polarization in complex scattering media, respectively. Figure 3(c) shows a reconstructed object image using conventional GI without any scattering media in the optical path for a comparison. It is illustrated that the GI is unable to visually render any information related to the sample, since dynamic scaling factors break the correlation relationship between illumination patterns and the collected single-pixel light intensities. The application of CPGI with dual polarization can facilitate the elimination of the effect of dynamic scaling factors, thereby achieving high-resolution

reconstruction (i.e., a line width of 70.15 μm). Here, contrast-to-noise ratio (CNR) [27] is further used to evaluate the reconstruction quality with signal area (red box) and background area (green box) indicated in Fig. 3(c). To ensure consistency and rationality, the same areas are defined to evaluate the experimental results. The CNR in Fig. 3(c) is 5.73, and the CNR in Fig. 3(a) is 0.56. The CNR in Fig. 3(b) is 6.17 which is even higher than that in Fig. 3(c). It is experimentally demonstrated that the proposed method is feasible and effective for high-resolution and high-contrast ghost reconstruction in complex and dynamic scattering environments.

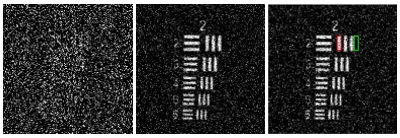

Fig. 3. Experimental results: (a) a reconstructed object image obtained by using conventional GI through dynamic and complex scattering media, (b) a reconstructed object image obtained by using the proposed CPGI with dual polarization through dynamic and complex scattering media, and (c) a reconstructed object image obtained by using conventional GI without any scattering media in the optical path for a comparison. Here, the dynamic and complex scattering environment is established using 5-ml skimmed milk (diluted with 200-ml clean water) and a stirring speed of 500.0 rpm.

Figures 4(a)–4(f) show the experimental results to illustrate how the proposed CPGI with dual polarization withstands dynamic and complex scattering. Figure 4(a) shows the collected single-pixel light intensities in the s-light and p-light paths. Here, a normalization operation is conducted for comparison among the series of collected single-pixel light intensities. Since skimmed milk is continuously dripped into water tank in experiments, a dynamic change of turbidity occurs and the collected single-pixel light intensities decrease. Since the same intensity changes are created in the s-light and p-light paths using the designed optical setup (i.e., a common path with dual polarization), the series of dynamic scaling factors can be fully corrected in Eq. (4), as shown in Fig. 4(b). The corrected single-pixel light intensities obtained by using the proposed CPGI with dual polarization renders a Gaussian distribution, as shown in Fig. 4(e). However, the collected single-pixel light intensities corresponding to the p-light and s-light paths cannot satisfy a Gaussian distribution, as shown in Figs. 4(c) and 4(d). To further illustrate performance of the developed CPGI with dual polarization, Fig. 4(f) shows the profiles along a line of the reconstructed object images. Three peaks corresponding to the three vertical bars in Group 2 Element 6 are clearly observed. High resolution (i.e., a line width of 70.15 μm) is achieved by using the proposed method in dynamic and complex scattering environments. It is demonstrated that the proposed CPGI with dual polarization is feasible and effective.

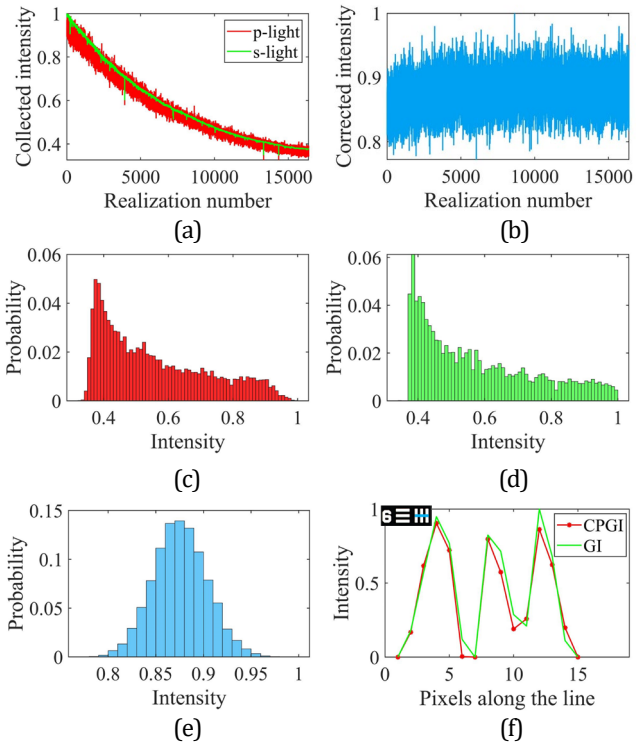

Fig. 4. The proposed CPGI with dual polarization through dynamic and complex scattering media: (a) the collected single-pixel light intensities in the p-light and s-light paths, (b) the corrected single-pixel light intensities, (c) a probability distribution of the collected single-pixel light intensities in p-light path, (d) a probability distribution of the collected single-pixel light intensities in s-light path, (e) a probability distribution of corrected single-pixel light intensities, and (f) the profiles along a line (indicated in the inset) of the reconstructed object images respectively obtained by using the proposed CPGI with dual polarization through dynamic and complex scattering media and conventional GI without any scattering media in the optical path.

To illustrate the reliability of the proposed CPGI with dual polarization, optical experiments were further conducted utilizing the varying volumes of skimmed milk and different stirring speeds. The CNR is also calculated to conduct a quantitative comparison between the CPGI with dual polarization and GI in complex media. Group 2 of the USAF 1951 resolution target is tested. Figure 5(a) shows experimental results using the proposed CPGI with dual polarization and conventional GI, when 3.0, 5.0, 7.0, 9.0, 11.0, 13.0, 15.0, 17.0, 30.0 and 50.0-ml skimmed milk to be individually diluted with 200-ml clean water is respectively used and continuously dripped in experiments. The stirring speed is 500.0 rpm. It is illustrated that the proposed CPGI with dual polarization is effective and reliable in correcting a series of dynamic scaling factors, leading to high-quality imaging (i.e., high CNRs). However, the GI is unable to render valid information related to the target, and the CNR values always remain low. It is worth noting that when milk volume is 30.0 ml or above, the collected single-pixel light intensities are low (~0.030 V at 30.0-ml milk). For a comparison, the collected single-pixel light intensity is ~0.027 V in the absence of laser. It is indicated that when the volume of milk is large, effective light intensity collected will be submerged in noise rather than being attributed to performance limit of the proposed

CPGI with dual polarization. This also illustrates why the CNR values of the reconstructed object images using the proposed CPGI decrease, when 30.0 or 50.0-ml milk is used in experiments. Different stirring speeds of 300.0, 500.0, 700.0, 900.0, 1100.0, 1300.0 and 1500.0 rpm are also employed to verify the proposed CPGI with dual polarization, as shown in Fig. 5(b). Here, the volume of skimmed milk is 5.0 ml diluted with 200-ml clean water. The proposed CPGI with dual polarization always shows excellent performance with high CNR values. Therefore, it is demonstrated that the developed CPGI with dual polarization exhibits high robustness and high reliability in complex and dynamic scattering environments.

Other targets are further tested using the proposed CPGI with dual polarization in dynamic and complex scattering environments, and experimental results are shown in Figs. 6(a)–6(d). Feasibility and effectiveness of the proposed CPGI with dual polarization are also verified, and the series of dynamic scaling factors is effectively corrected to realize high-quality imaging in dynamic and complex scattering environments.

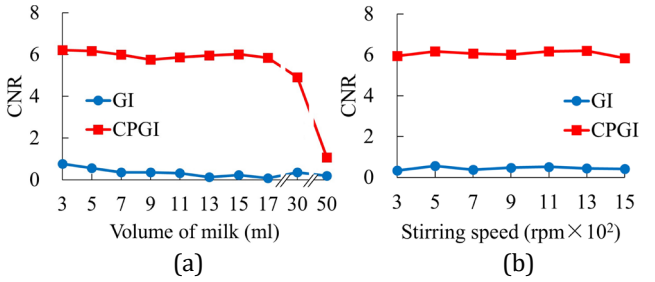

Fig. 5. Experimental results obtained by using the proposed CPGI with dual polarization and GI: (a) effect of the milk volume on the CNR of the reconstructed object images, and (b) effect of the stirring speed on the CNR of the reconstructed object images.

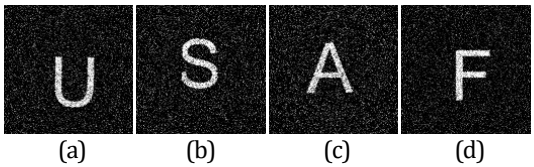

Fig. 6. Experimental results: (a)-(d) the reconstructed object images obtained by using the proposed CPGI with dual polarization. In experiments, 5.0-ml skimmed milk diluted with 200-ml clean water was continuously dripped into water tank and a stirring speed of 500.0 rpm was used.

In conclusion, we have designed a common path with dual polarization in GI to accurately correct a series of dynamic scaling factors in dynamic and complex scattering media. This new approach does not need to employ complex algorithms, and adopts the strategy of an optical design to facilitate the realization of high-quality imaging through complex scattering media. A simplified optical setup and a simple correlation algorithm are applied. Many scattering media are isotropic (e.g., smoke) and generally have little effect on the polarization rotation or depolarization of photons. These characteristics make the proposed CPGI with dual polarization to be promising in real-world scenarios, especially through complex media. It can be expected that the proposed method with a common-path setup and dual polarization could open an avenue for GI in various applications.

Funding. Hong Kong Research Grants Council (15224921, 15223522); GuangDong Basic and Applied Basic Research Foundation (2023A1515010831, 2022A1515011858); The Hong Kong Polytechnic University (1-WZ4M, 1-CDJA).

REFERENCES

1. J. Yang, Q. He, L. Liu, Y. Qu, R. Shao, B. Song, and Y. Zhao, Light.: Sci. Appl. **10**, 149 (2021).
2. U. Najar, V. Barolle, P. Balondrade, M. Fink, C. Boccara, and A. Aubry, Nat. Commun. **15**, 7349 (2024).
3. T. B. Pittman, Y. H. Shih, D. V. Strekalov, and A. V. Sergienko, Phys. Rev. A **52**, R3429 (1995).
4. Y. Zhang, W. Li, H. Wu, Y. Chen, X. Su, Y. Xiao, Z. Wang, and Y. Gu, Opt. Commun. **441**, 45 (2019).
5. P. Ryczkowski, M. Barbier, A. T. Friberg, J. M. Dudley, and G. Genty, Nat. Photon. **10**, 167 (2016).
6. B. I. Erkmen, J. Opt. Soc. Am. A **29**, 782 (2012).
7. C. Zhao, W. Gong, M. Chen, E. Li, H. Wang, W. Xu, and S. Han, Appl. Phys. Lett. **101**, 141123 (2012).
8. M. J. Sun, M. P. Edgar, G. M. Gibson, B. Sun, N. Radwell, R. Lamb, and M. J. Padgett, Nat. Commun. **7**, 12010 (2016).
9. Y. Xu, L. Lu, V. Saragadam, and K. F. Kelly, Nat. Commun. **15**, 1456 (2024).
10. S. Yuan, L. Wang, X. Liu, and X. Zhou, Opt. Lett. **45**, 3917 (2020).
11. W. Huang, W. Tan, H. Qin, J. Wang, Z. Huang, X. Huang, X. Fu, and Y. Bai, J. Opt. Soc. Am. B **40**, 1696 (2023).
12. L. Olivieri, J. S. T. Gongora, L. Peters, V. Cecconi, A. Cutrona, J. Tunesi, R. Tucker, A. Pasquazi, and M. Peccianti, Optica **7**, 186 (2020).
13. S. Han, H. Yu, X. Shen, H. Liu, W. Gong, and Z. Liu, Appl. Sci. **8**, 1379 (2018).
14. Y. Xiao, L. Zhou, and W. Chen, Opt. Lett. **47**, 3692 (2022).
15. Y. Cao, Y. Xiao, Z. Pan, L. Zhou, and W. Chen, Opt. Express **30**, 36464 (2022).
16. T. Wang, M. Chen, H. Wu, H. Xiao, S. Luo, and L. Cheng, Appl. Opt. **60**, 6950 (2021).
17. D. Shi, C. Fan, P. Zhang, J. Zhang, H. Shen, C. Qiao, and Y. Wang, Opt. Express **20**, 27992 (2017).
18. Y. Yu, M. Hou, C. Hou, Z. Shi, J. Zhao, and G. Cui, Sensors **23**, 9002 (2023).
19. W. Yu, S. A. A. Shah, D. Li, K. Guo, B. Liu, Y. Sun, Z. Yin, and Z. Guo, Opt. Laser Technol. **169**, 110024 (2024).
20. Z. Sun, T. Tian, S. Oh, J. Wang, G. Cheng, and X. Li, Chin. Opt. Lett. **21**, 081101 (2023).
21. D. Li, C. Xu, L. Yan, and Z. Guo, Opt. Express **30**, 17909 (2022).
22. W. Gong and S. Han, Opt. Lett. **36**, 394 (2011).
23. Y. Chen, Z. Sun, C. Li, and X. Li, Opt. Laser Technol. **167**, 109735 (2023).
24. Z. Gao, X. Cheng, K. Chen, A. Wang, Y. Hu, S. Zhang, and Q. Hao, IEEE Photon. J. **12**, 1 (2020).
25. Y. Peng and W. Chen, Opt. Lett. **48**, 4480 (2023).
26. L. Zhou, Y. Xiao, and W. Chen, Opt. Express **31**, 23027 (2023).
27. B. Redding, M. A. Choma, and H. Cao, Nat. Photon. **6**, 355 (2012).

References with titles

1. J. Yang, Q. He, L. Liu, Y. Qu, R. Shao, B. Song, and Y. Zhao, "Anti-scattering light focusing by fast wavefront shaping based on multi-pixel encoded digital-micromirror device," Light.: Sci. Appl. 10, 149 (2021).
2. U. Najar, V. Barolle, P. Balondrade, M. Fink, C. Boccara, and A. Aubry, "Harnessing forward multiple scattering for optical imaging deep inside an opaque medium," Nat. Commun. 15, 7349 (2024).
3. T. B. Pittman, Y. H. Shih, D. V. Strekalov, and A. V. Sergienko, "Optical imaging by means of two-photon quantum entanglement," Phys. Rev. A 52, R3429 (1995).
4. Y. Zhang, W. Li, H. Wu, Y. Chen, X. Su, Y. Xiao, Z. Wang, and Y. Gu, "High-visibility underwater ghost imaging in low illumination," Opt. Commun. 441, 45 (2019).
5. P. Ryczkowski, M. Barbier, A. T. Friberg, J. M. Dudley, and G. Genty, "Ghost imaging in the time domain," Nat. Photon. 10, 167 (2016).
6. B. I. Erkmen, "Computational ghost imaging for remote sensing," J. Opt. Soc. Am. A 29, 782 (2012).
7. C. Zhao, W. Gong, M. Chen, E. Li, H. Wang, W. Xu, and S. Han, "Ghost imaging lidar via sparsity constraints," Appl. Phys. Lett. 101, 141123 (2012).
8. M. J. Sun, M. P. Edgar, G. M. Gibson, B. Sun, N. Radwell, R. Lamb, and M. J. Padgett, "Single-pixel three-dimensional imaging with time-based depth resolution," Nat. Commun. 7, 12010 (2016).
9. Y. Xu, L. Lu, V. Saragadam, and K. F. Kelly, "A compressive hyperspectral video imaging system using a single-pixel detector," Nat. Commun. 15, 1456 (2024).
10. S. Yuan, L. Wang, X. Liu, and X. Zhou, "Forgery attack on optical encryption based on computational ghost imaging," Opt. Lett. 45, 3917 (2020).
11. W. Huang, W. Tan, H. Qin, J. Wang, Z. Huang, X. Huang, X. Fu, and Y. Bai, "Edge detection based on ghost imaging through biological tissue," J. Opt. Soc. Am. B 40, 1696 (2023).
12. L. Olivieri, J. S. T. Gongora, L. Peters, V. Cecconi, A. Cutrona, J. Tunesi, R. Tucker, A. Pasquazi, and M. Peccianti, "Hyperspectral terahertz microscopy via nonlinear ghost imaging," Optica 7, 186 (2020).
13. S. Han, H. Yu, X. Shen, H. Liu, W. Gong, and Z. Liu, "A Review of Ghost Imaging via Sparsity Constraints," Appl. Sci. 8, 1379 (2018).
14. Y. Xiao, L. Zhou, and W. Chen, "High-resolution ghost imaging through complex scattering media via a temporal correction," Opt. Lett. 47, 3692 (2022).
15. Y. Cao, Y. Xiao, Z. Pan, L. Zhou, and W. Chen, "High-fidelity temporally-corrected transmission through dynamic smoke via pixel-to-plane data encoding," Opt. Express 30, 36464 (2022).
16. T. Wang, M. Chen, H. Wu, H. Xiao, S. Luo, and L. Cheng, "Underwater compressive computational ghost imaging with wavelet enhancement," Appl. Opt. 60, 6950 (2021).
17. D. Shi, C. Fan, P. Zhang, J. Zhang, H. Shen, C. Qiao, and Y. Wang, "Adaptive optical ghost imaging through atmospheric turbulence," Opt. Express 20, 27992 (2017).
18. Y. Yu, M. Hou, C. Hou, Z. Shi, J. Zhao, and G. Cui, "Self-modulated ghost imaging in dynamic scattering media," Sensors 23, 9002 (2023).
19. W. Yu, S. A. A. Shah, D. Li, K. Guo, B. Liu, Y. Sun, Z. Yin, and Z. Guo, "Polarized computational ghost imaging in scattering system with half-cyclic sinusoidal patterns," Opt. Laser Technol. 169, 110024 (2024).
20. Z. Sun, T. Tian, S. Oh, J. Wang, G. Cheng, and X. Li, "Underwater ghost imaging with pseudo-bessel-ring modulation pattern," Chin. Opt. Lett. 21, 081101 (2023).
21. D. Li, C. Xu, L. Yan, and Z. Guo, "High-performance scanning-mode polarization based computational ghost imaging (SPCGI)," Opt. Express 30, 17909 (2022).
22. W. Gong and S. Han, "Correlated imaging in scattering media," Opt. Lett. 36, 394 (2011).
23. Y. Chen, Z. Sun, C. Li, and X. Li, "Computational ghost imaging in turbulent water based on self-supervised information extraction network," Opt. Laser Technol. 167, 109735 (2023).
24. Z. Gao, X. Cheng, K. Chen, A. Wang, Y. Hu, S. Zhang, and Q. Hao, "Computational ghost imaging in scattering media using simulation-based deep learning," IEEE Photon. J. 12, 1 (2020).
25. Y. Peng and W. Chen, "Learning-based correction with Gaussian constraints for ghost imaging through dynamic scattering media," Opt. Lett. 48, 4480 (2023).
26. L. Zhou, Y. Xiao, and W. Chen, "High-resolution self-corrected single-pixel imaging through dynamic and complex scattering media" Opt. Express 31, 23027 (2023).
27. B. Redding, M. A. Choma, and H. Cao, "Speckle-free laser imaging using random laser illumination," Nat. Photon. 6, 355 (2012).